Nuclear Inst. and Methods in Physics Research, A 1047 (2023) 167782

Contents lists available at ScienceDirect

Nuclear Inst. and Methods in Physics Research, A

journal homepage: www.elsevier.com/locate/nima

Performance of a resistive micro-well detector with capacitive-sharing strip anode readout

Kondo Gnanvo [a,*], Nilanga Liyanage [a], Bertrand Mehl [b], Rui de Oliveira [b]

[a] University of Virginia, Department Of Physics, Charlottesville VA 22903, USA
[b] CERN Esplanade des Particules 1 P.O. Box 1211 Geneva 23, Switzerland

ARTICLE INFO

Keywords:
Capacitive-sharing readouts
Spatial resolution
GEM
μRWELL
Micromegas
MPGD
(X-Y) strip readout

ABSTRACT

The present study is carried out to demonstrate a new type of high-performance readout structure with low readout channel count developed for large-area micro pattern gaseous detectors. The structure exploits capacitive coupling between a vertical stack of 5 μm thick copper pad layers sandwiched between 50 μm thick polyimide foils to simultaneously transfer and spread the avalanche charges from the gaseous detector's amplification structure to several strips or pads in the anode readout plane. The unique feature of the lateral spread of the avalanche charge size on several readout strips or pads is possible owing to well-defined configuration and sizes of the pads in layers of the vertical stack. This is known as a "capacitive-sharing" readout structure and this opens the door for high spatial resolution performance with low readout channel counts for large-area Micro Pattern Gaseous Detectors. Capacitive-sharing readout structures are fabricated using standard printed circuits boards manufacturing process. The concept is highly versatile as it can easily be implemented in any type of Micro Pattern Gaseous Detector's amplification structure (Gas Electron Multipliers, micro-mesh gaseous structures, resistive micro-well detectors) and with a wide range of readout patterns (pads, strips, zigzags etc.). The technology also has a high degree of flexibility in terms of readout segmentation (pads or strip) pitch, with minimum impact on spatial resolution performances. The present study provides a detailed description of the capacitive-sharing readout concept and discusses a small resistive micro-well detectors prototype assembled with a two-dimensional capacitive-sharing strip readout structure as a proof of concept and with strip pitch of 800 μm in both X and Y direction. The prototype was characterized in electron beam in the Hall D Beam Test setup at Jefferson Lab and a spatial resolution of (60 ± 1) μm was achieved for both X and Y strips with an efficiency of (98.0 ± 0.9) % at the plateau and a signal arrival time jitter between neighboring strips less (6.00 ± 0.04) ns. Finally, we explore new ideas to expand the concept of capacitive-sharing readout structures to large particle detectors for future large scale particle physics experiments.

1. Introduction

Micro-pattern gaseous detector (MPGD) technologies such as Gas Electron Multiplier (GEM) [1], Micro-Mesh Gaseous Structure (Micromegas) [2], Resistive Micro-Well (μRWELL) [3] or Thick GEM (THGEM) [4] are widely used for tracking, particle identification (PID), calorimetry in high energy physics (HEP) and nuclear physics (NP) experiments across the world. These gaseous detector technologies typically combine an electron multiplication device with high segmentation strip or pad pick-up electrodes used as anode readout PCB to provide precision particle position measurement. For example, the 2D strip (X-Y) readout of the triple-GEM trackers used in the COMPASS experiment [5–7] at CERN can achieve a spatial resolution of ∼50 μm with a strip segmentation of 400 μm pitch. Alternately, for applications that require less stringent space point resolution, a pad readout with pitch of a few mm is typically preferred and provide space point resolution equal to the pad pitch divided by $\sqrt{12}$. Better spatial resolution performance would require smaller pad sizes resulting in a higher number of electronic channels. For large-area tracking systems, such as the detectors under consideration for future HEP and NP colliders and fixed targets experiments [8–11], a large number of thin strips or pads creates a whole set of challenges not only in terms of the high cost of large number of readout electronics, but also in terms of detector integration, cooling scheme for the electronics, cabling and other services. A large number of electronics channels also has an adverse impact in terms of dead area in detector acceptance, additional material thickness affecting multiple coulomb scattering as well as radiation hardness issues, especially when the front end cards have to be mounted directly on the detectors.

* Correspondence to: Thomas Jefferson National Accelerator Facility (Jefferson Lab), Newport News VA 23606, USA.
E-mail address: kagnanvo@jlab.org (K. Gnanvo).

https://doi.org/10.1016/j.nima.2022.167782
Received 7 May 2022; Received in revised form 1 November 2022; Accepted 7 November 2022
Available online 17 November 2022
0168-9002/

Several R&D efforts [12–14] are ongoing to develop low channel counts and high-performance readout PCB structures for large-area MPGDs. One such development is the resistive anode readout [14–16]. This consists of an additional thin resistive layer directly on top of pick-up strip or pad electrodes of the readout PCB, designed to laterally spread electron charge from the amplification layer (MPGD) over several strips or pads to allow precise position reconstruction of the particle using a center of gravity (COG) or a more complex algorithm. The development of resistive readout structures is particularly advanced for TPC application using an MPGD end cap readout plane. These studies demonstrated that a spatial resolution of ∼60 μm can be achieved with 3×3 mm^2 size pad readout [14]. Another approach is the development of "zigzag" or "chevron" readout [12,13]. The idea in this case, is to modify standard square pads or straight strips into a chevron shape geometry to improve further the charge sharing between neighboring pads or strips. Spatial resolution performance in the range of 50 to 70 μm has been demonstrated with 2 mm pitch "zigzag" pad readout on MPGD prototypes [12], comparable to the performance achieved with standard "COMPASS"style (X-Y) strip readout [5] with a strip pitch of 400 μm. However, the implementation of zigzag or resistive-sharing readout structures for large-area tracking detector faces several critical challenges. Resistive-sharing readout structures require very good uniformity of the thickness of the resistive layer over large-area to ensure uniform pad response function across the detector. The techniques currently available for producing resistive layers such as sputtering or screen printing, do not allow good control of the thickness uniformity of commonly used resistive foil such as diamond-like carbon (DLC) foils. Careful mapping of the layer non-uniformity and calibration of the pad response function of detector are necessary for each individual detector to correct or compensate for the non-uniformity and non-linearity. This approach is not practical for use in large-area, mass production detectors for large scale particle physics experiments.

Another critical challenge associated with resistive-sharing readout structures is the large time delay between pads from the same event cluster participating in the charge sharing due to the time constant characteristics of the resistive layer. The issue has been extensively studied and reported in literature, showing a peaking time delay as large as 1 μs between neighboring strips that are sharing charge [16]. This constitutes a severe limitation for using this type of charge-sharing readout in moderate and high background environment where mitigation of pile-up and optimization of rate capability are crucial. This also creates additional challenges in the selection of the characteristics of front-end electronics to read out the detectors. The resistive layers are also used for spark protection for MPGD detectors such as Micromegas and μRWELL detectors. So a compromise is always necessary between the optimal surface resistivity of the DLC for the detector to operate in a spark-free mode and ensure charge spread for high spatial resolution performance. Zigzag readout structures have been initially developed and optimized for 1D strip readout structures. Recent developments of 2D "zigzag" readout structures [17] have shown encouraging early performance but the development is still at an early stage. More importantly, the key geometric parameters that define the zigzag readout structures [18] are typically optimized for a given MPGD amplification structures and are not easily interchangeable between technologies. In addition, zigzag readout structures are technically complex structures that pose non-trivial challenges for the large-area fabrication of these structures.

In the current study, a novel concept of readout structure called the "capacitive-sharing readout structures" is presented. This technology allows charge transfer and charge sharing for large pitch (strip or pad) anode readout PCB layers using capacitive coupling between a stack of layers of pads. Capacitive-sharing readout structures offer a high-performance spatial resolution capability with significant reduction of electronic channels required to read out large-area MPGD trackers. The new readout structures are inherently flexible, versatile and easy to implement in different types of readout pattern (straight strips, zigzag strips, pad) and with all MPGD amplification devices (GEM, Micromegas, μRWELL). The fabrication of capacitive-sharing readout is based on standard PCB techniques, making the technology a low risk, cost-effective option for large-area MPGD detectors.

In Section 2 of this paper, we introduce the concept of capacitive-sharing readout with a detailed description of the principle. In Section 3, we present the development of a small (10 cm × 10 cm) μRWELL prototype with 800 μm pitch X-Y strip readout based on this capacitive-sharing concept. In Section 4, the basic performance characteristics of the prototype measured in beam test at Jefferson Lab are discussed. The spatial resolution performance is reported in Section 6. Finally, in Section 7, we introduce new ideas to improve the performance and expand the capabilities of capacitive-sharing readout structures, before the conclusion and a brief survey of future potential applications for these new readout structures.

2. Concept of capacitive-sharing readout structures

2.1. Charge sharing via capacitive coupling between pad layers in a vertical stack.

The basic concept of capacitive-sharing readout structures is shown in Fig. 1. The figure shows a vertical stack of layers; each layer consists of 5 μm copper (Cu) pads deposited on 50 μm polyimide (Kapton or Apical) foils. The Cu-polyimide layers are based on the same base material used for the production of GEM foils. The stack of several such layers can be viewed, in a simple approximation, as a set capacitors in series along the vertical direction as a way to simply describe how charge are transferred from one layer to another. The more accurate model describing the actual equivalent circuit is more complex than a linear capacitor network and is under development and will be presented in a future publication. The Cu on each layer is chemically etched into pads with their pitch doubling in size from one layer$_i$ to the layer$_{i+1}$ underneath it.

The layer at the bottom of the stack is the actual *"readout layer"*, the one connected to the front-end amplifiers cards of the readout electronics. The readout layer can be pad or strip readout or any other type of readout pattern. Above the readout layer, is the stack of *"transfer layers"* responsible for the propagation of the incoming signal via a cascade of capacitive coupling process from the amplification structure to the readout layer. The layer in grey at the top of the first transfer layer in Fig. 1 is the resistive layer which is a nanometer scale diamond-like carbon (DLC) layer required for the draining of incoming charges to the ground. The yellow highlighting illustrates the incoming electron charge cloud from the GEM amplification and mechanism of charge spread over neighboring pads of increasing size during the transfer from top pad layer up to readout layer via capacitive coupling.

The transfer layers always consists of pads with the geometrical center of each pad in a given layer$_i$ of the stack, alternatively centered with a larger pad in layer$_{i+1}$ underneath it and aligned with a boundary between two adjacent larger pads of layer$_{i+1}$. This principle is shown in Fig. 2. The relative alignment of the pads from one transfer layer to the other, combined with doubling of pad size from layer to layer, is the mechanism by which charge induced on any two neighboring pads of layer$_i$ is transferred via capacitive coupling to two neighboring pads of layer$_{i+1}$ below, with twice the pad size. The signal propagates vertically through the transfer layers up to the readout layer via capacitive coupling while transversely spreading over pads of increasing size. This is the unique and characteristic feature of this novel readout structure concept that is referred to as *"capacitive-sharing readout"* in this study. With this simple design, a pad or strip readout plane with capacitive-sharing feature (transfer pad layers) only requires a small number of large readout pads or strips to provide excellent spatial resolution performance with an MPGD. For n layers, the number of readout pads or strips along one axis of the readout plane, connected

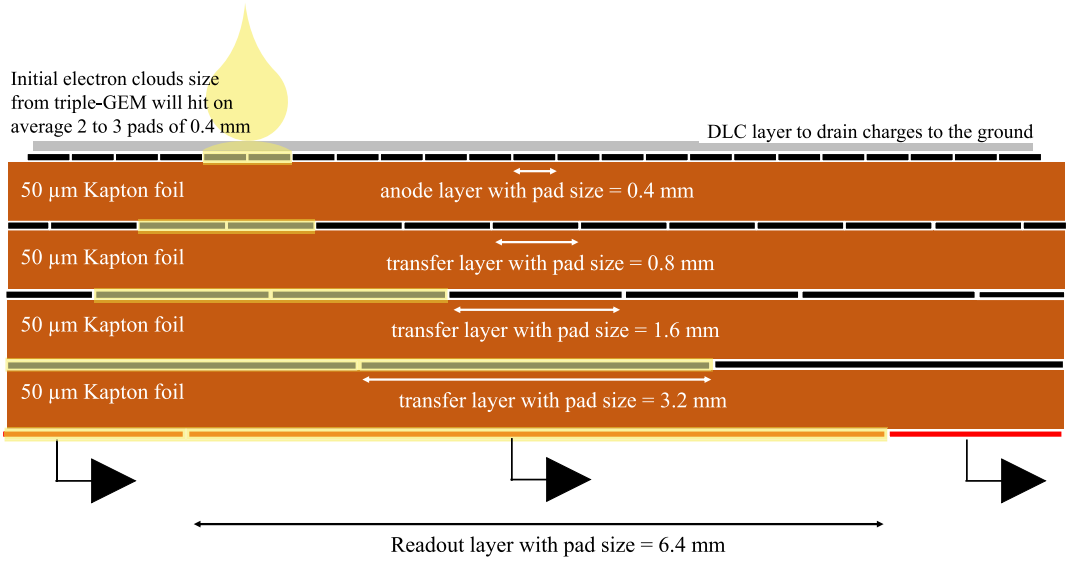

Fig. 1. Cross-sectional view of capacitive-sharing pad readout showing the transfer layers *(black pads)*; the readout layer with 6.4 mm × 6.4 mm pads *(red)*; the grey layer on top is the DLC resistive layer and the yellow highlighting illustrates the mechanism of charge spread over neighboring pads during the propagation of the signal from the top to the readout layer at the bottom.

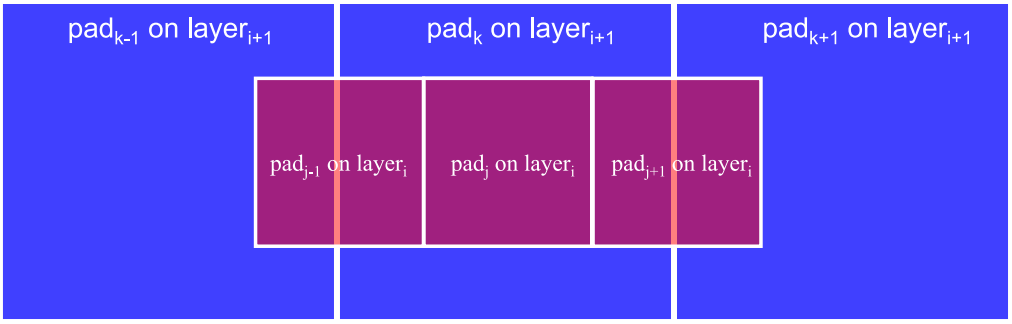

Fig. 2. Cartoon illustration of the charge sharing scheme via capacitive coupling from small pads to larger pads of two transfer layers.

to the front end electronics is only a fraction 1/n of the number of pads along the same axis of the first transfer layer collecting the incoming signal from the MPGD amplification structure. In essence, the pad size of this first transfer layer (layer$_1$) defines the spatial resolution performance of the readout plane and the pad size of readout layer (layer$_n$) defines the total number of electronic channels required to read out the detector plane. Therefore, unlike zigzag or resistive-sharing readout structures, [12,14,16], the spatial resolution performance of the capacitive-sharing readout structures is, in the first approximation, independent of the pitch of the strip readout or the size of pad readout segmentation as we will demonstrate in Section 6 of this paper.

2.2. Versatility of capacitive-sharing readout structures.

As mentioned in the introduction Section 1, the capacitive-sharing readout concept described in Section 2.1 is extremely versatile and could be coupled with all types of MPGD amplification structures e.g. GEM, Micromegas or µRWELL with any anode readout patterns such as pads, 2D strip, 3-coordinate (X-Y-U) strip, as well as zigzag readout structures [18]. In addition, capacitive-sharing offers the flexibility to select pad size or strip pitch over a large range without compromising the spatial resolution performance of the MPGD. This gives to the user the possibility to adjust the characteristics of the detector readout structure to specific requirements such as reduction of the number electronic channels or services related constraints such as cabling, cooling and shielding related to integration of MPGD trackers into large and complex detector systems at colliders or fixed targets particle physics experiments.

3. µRWELL prototype with capacitive-sharing X-Y strip readout structure

As a proof of concept, a small (10 cm × 10 cm) µRWELL PCB with X-Y strip capacitive-sharing readout layer was designed and fabricated in collaboration with the PCB workshop at CERN. The final assembly of the detector with the gas volume and cathode layer was completed and the initial testing on a cosmic setup was done in the MPGD Lab at the University of Virginia before a more extensive test in beam in Experimental Hall D at Jefferson Lab in Fall 2021. A picture of the capacitive-sharing readout µRWELL PCB composite is shown in top left of Fig. 3, with a zoomed-in view of the X-Y strip layer arrangement at the bottom left, and the cross section views of the layout of the µRWELL amplification stage, the capacitive-sharing layer stack along both X and Y axes shown at the right.

The µRWELL PCB is composed of three parts:

- **The amplification device:** The amplification stage of the detector is the 55 µm thick µRWELL foil, a single copper-clad polyimide foil featuring a high density of conical-shaped holes, similar to a GEM foil, with a diameter of 70 µm at the top copper side, 50 µm at the bottom, and a pitch of 140 µm. A thin DLC layer (≤ 100 µm) with a surface resistivity of ∼20 MΩ / □ is sputtered on the bottom side of the polyimide prior to the chemical etching process that creates the amplification holes of the µRWELL. Finally, the µRWELL/DLC foil is glued to the readout PCB layer. A set of conductive strips at the perimeter of the DLC are used to drain the charges from the amplification stage to ground.

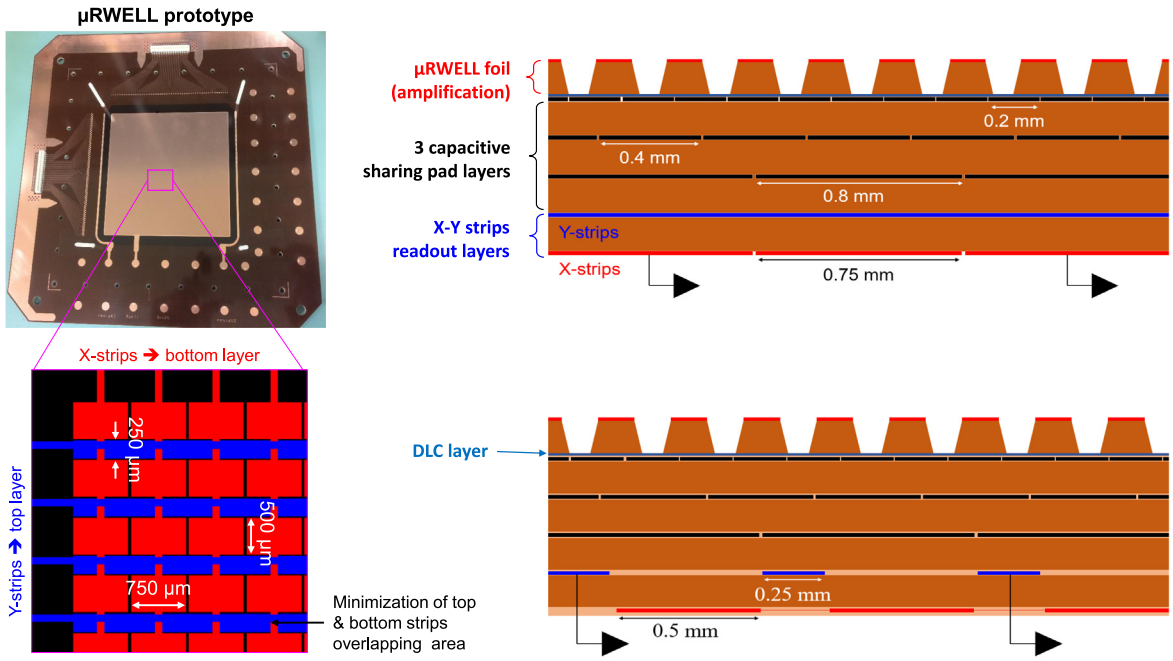

Fig. 3. Capacitive-sharing X-Y readout PCB for μRWELL prototype. *Left, top:* Picture of the PCB layer of μRWELL detector prototype with a single 130-pins Panasonic connector per axis for 2 × 128 (X-Y) strip readout. *Left, bottom:* a zoom-in view of the Gerber file showing the X-Y strip readout configuration with the Y-strips *(in red)* and X-strips *(in blue)*. *Right:* Cross sectional view of the three capacitive-sharing pad transfer layers and the two readout strip layers along X and Y axis.

- **The capacitive-sharing transfer pad layers:** The capacitive-sharing structure is based on the same concept described in Section 2.1 but with only a 3-layer stack for transfer layers for this prototype, with pad sizes of 200 μm ×200 μm, 400 μm ×400 μm, 800 μm × 800 μm for the three transfer layers. The stack is [art of the readout PCB stack on top of which the μRWELL/DLC foil is glued.
- **The X-Y strip readout layers:** X- and Y-strips are on the last two layers of the PCB stack, below the 3 capacitive-sharing transfer layers. The Y-strips (top readout strips), shown in blue on the Gerber view (in bottom left of Fig. 3), have a strip width of 250 μm. The X-strips (bottom strip layer), in red, sit 50 μm below the Y-strips, separated by a polyimide layer and have a width of 750 μm. The top and bottom strips sit respectively 25 μm and 50 μm below the third transfer layer (800 μm × 800 μm pads), meaning that the coupling capacitance of the top strips is twice that of the bottom strips. The bottom strips need to be wider than the width of the top strips to create equal charge sharing between the top and bottom strips. The chosen width ratio (250 μm/750 μm) for this prototype was guided by our previous experience with the COMPASS readout design which has similar X-Y strip with a pitch of 400 μm for both X- and Y-strip, but widths of 80 μm and 340 μm, respectively. We will discuss in Section 4 the impact of the charge-sharing ratio on spatial resolution performance and will propose the adjustment on X- and Y-strip width ratio for future prototypes.

The μRWELL detector assembly is completed after the cathode foil is added with a 3 mm drift distance and the stack is inserted in the gas box enclosure and sealed for gas tightness with a set of O-rings and gas box lid. The prototype is tested first in dry nitrogen with 600 V applied to the μRWELL foil and the measured leakage current is less than 10 nA. After successfully completing this HV test, the prototype is ready to operated in an Argon - Carbon Dioxide (Ar:CO_2 - 80:20) gas mixture. We set the maximum voltage applied to the μRWELL foil to HV = 580 V when operating the chamber, that is 20 V lower than the maximum voltage during the test with dry nitrogen gas.

4. Studies in beam test of μRWELL prototype.

4.1. Beam test setup in Hall D at Jefferson Lab

The X-Y capacitive-sharing μRWELL prototype was installed in a telescope with four standard COMPASS X-Y triple-GEM trackers in the electron arm area of the Hall D Pair Spectrometer (PS) at Jefferson Lab during the CEBAF fall run in August 2021. The X-Y capacitive-sharing μRWELL prototype was installed in a telescope with four standard COMPASS X-Y triple-GEM trackers in the electron arm area of the Hall D Pair Spectrometer (PS) at Jefferson Lab during the CEBAF fall run in August 2021.

The layout of the PS test beam area is shown in Fig. 4. The PS delivers a clean electron beam at a rate of 10 kHz and in an energy range of 3 to 6 GeV from γ conversion from the main GLUeX photon beam line. The converted electrons are bent in the horizontal direction by a 1.8T dipole, in a narrow band of ∼40 cm range in the horizontal plane and 5 mm in the vertical direction. In the setup shown in the right of Fig. 4, the μRWELL prototype is sandwiched between two sets of two standard COMPASS X-Y triple-GEM trackers for precise tracking of the electrons. All chambers in the setup were operated with an Ar:CO_2 80:20 gas mixture and read out with the APV25 electronics [19] implemented in the Scalable Readout System (SRS) [20] developed by CERN RD51 collaboration. The ADC sampling rate was set at 50 ns during data acquisition. For each triggered event, nine APV25 time samples corresponding to a data window of 450 ns were recorded per readout channel. The SRS DAQ received the trigger from Hall D PS coincidence trigger to operate as a standalone system alongside the GLUeX main DAQ, however the SRS trigger rate was reduced to a maximum ∼1 kHz via software to avoid data corruption during data writing into the disk because of low performance SRS DAQ PC. DATE package was used to transfer the data via Gigabit Ethernet to the DAQ PC and amoreSRS, the SRS online monitoring and offline analysis software implementation in AMORE framework. Both DATE and AMORE packages have been developed by the CERN ALICE collaboration [21] and later adopted by RD51 collaboration for MPGD SRS readout system.

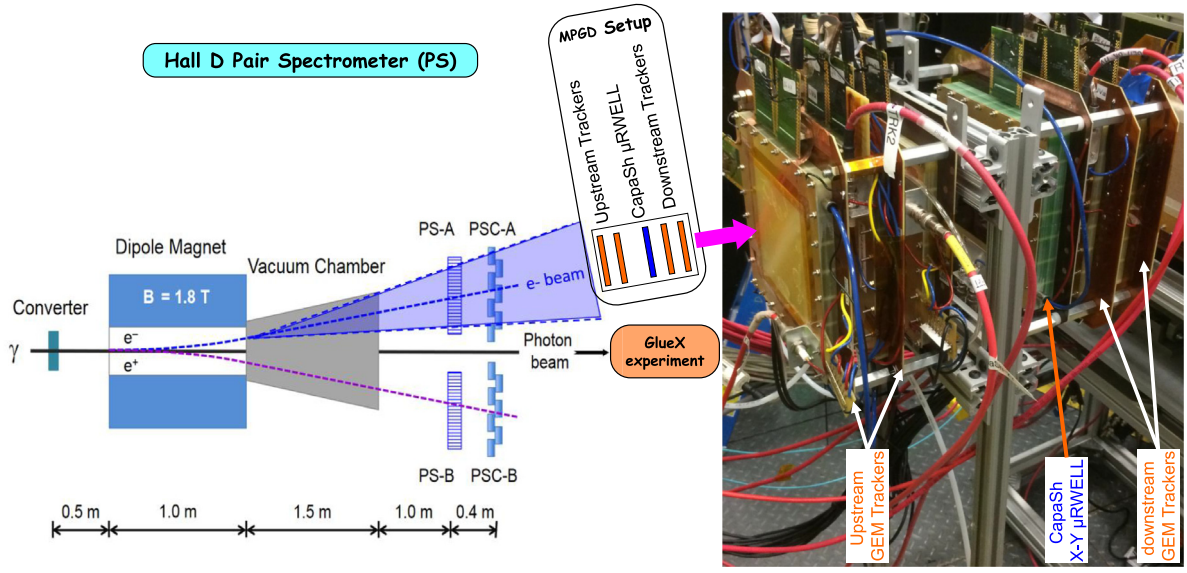

Fig. 4. Layout of the Pair Spectrometer (PS) in Experimental Hall D at Jefferson Lab *(left)*; the MPGD telescope with 4 COMPASS triple-GEM trackers and the capacitive-sharing µRWELL prototype under study installed in the electron arm of the PS *(right)*.

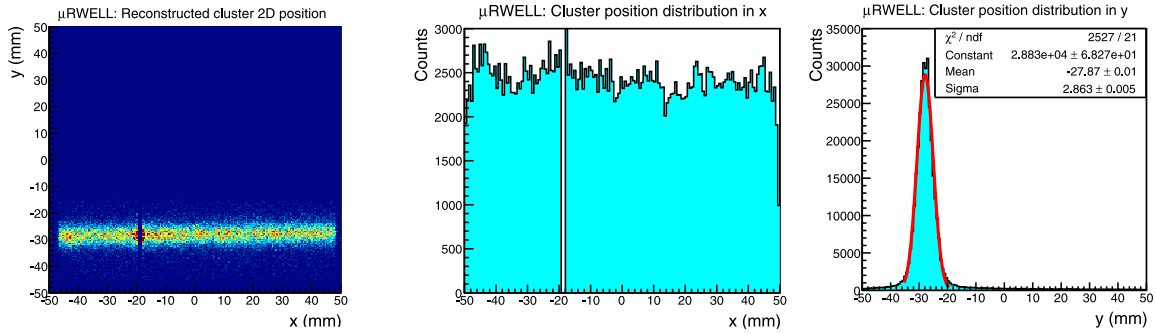

Fig. 5. Hall D PS electron beam profile reconstructed with the capacitive-sharing µRWELL prototype: 2D hit position map *(left)*; reconstructed hit position distribution in x *(middle)*; reconstructed hit position distribution in y *(right)*. The efficiency loss caused by two dead channels of the APV25 FE connected to the x-strips is shown on the left and middle plots at $x \sim -18$ mm.

4.2. Offline data analysis and PS electron beam profile

The primary goal for this beam test campaign was to evaluate the performances of capacitive-sharing readout structures with µRWELL detector with a focus on the detector efficiency and spatial resolution. Several voltage scan runs were taken with HV applied separately to the drift cathode and to the µRWELL amplification structure to evaluate the impact of the gain and drift electric field on efficiency, strip multiplicity and spatial resolution. The data are analyzed using the amoreSRS software package. The package includes the data decoder for the raw APV25 events, scripts for common mode correction pedestal offset subtraction and $5 \times \sigma_{ped}$ threshold cut for zero suppression, based on uploaded channel by channel APV25 pedestal mean and rms data from previously computed and stored in root files. Strips cluster and hit position information in x and y axes from each event are computed and correlated to reconstruct 2D hit positions. The profile of Hall D Pair Spectrometer electron beam is reconstructed with the hits in the µRWELL prototype as shown in the plots of Fig. 5. The electron beam has a narrow width (3 mm rms) along the y-axis in the vertical direction but covers the full 10 cm width of the detector in the horizontal direction (x-strips). The system is triggered by the electron/positron coincidence event of the pair spectrometer. The event multiplicity defined as the average number of charged particles producing hits in the detector for each triggered event is 1.04, resulting in a clean event data sample for the analysis.

5. Performance characteristics of the µ RWELL prototype

In beam test, two types of voltage scan studies were performed. The first was a voltage scan in the drift volume of the prototype by varying the voltage applied to the cathode from 875 to 1175 V by 25 V steps while the voltage applied to the µRWELL was fixed at 575 V. The voltage difference in the 3 mm drift region therefore increases from 300 to 600 V corresponding to an electric field in the drift volume varying from 1 to 2 kV/cm. In studies reported in the literature, µRWELL detector typically operates at electric field in the drift region lower than 1 kV/cm. For standard triple-GEMs, the typical electric field in the drift region is 2 to 2.5 kV/cm. So a range 1 to 2 kV/cm for the HV scan of the µRWELL prototype seems appropriate for this study. The second HV study was a voltage scan of the µRWELL amplification structure from 550 to 580 V by 5 V steps while keeping a fixed electric field of 1.33 kV/cm in the drift region. We have not performed a direct gain curve measurement as a function of the voltage applied to the µRWELL foil, however, a gain curve study of µRWELL detector has been performed and reported in [3]. A gain of 6000 is achieved for a voltage of 525 V in Ar:CO_2 - 70:30 gas mixture and based on the data of [3], this would result in a gain of $\sim 1.2 \times 10^4$ at 575 V. With the operating voltage on the µRWELL foil for this study of 575 V and the Ar:CO_2 gas mixture of 80:20, we expected a slightly higher gain than 1.2×10^4.

For each voltage setting, the analysis requires a minimum of 10k good tracks in all four GEM trackers. The µRWELL performance presented in this study where obtained for a 5 sigma pedestal cut to

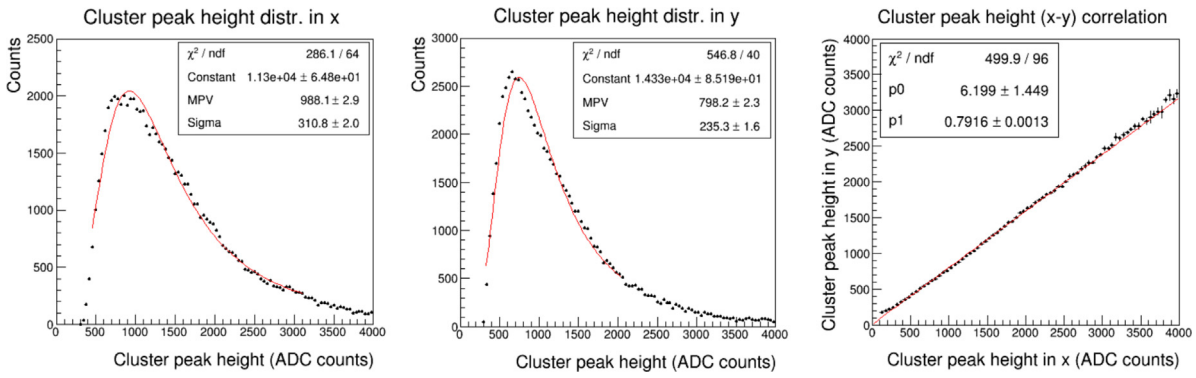

Fig. 6. Cluster ADC charge distribution in *x (left)* and in *y (center)*; the data are fitted to a Landau function *(red)*. Cluster charge-sharing correlation between x-strips vs. y-strips *(right)*.

μRWELL data for the zero suppression. We also produce efficiency plots for 3 sigma pedestal cut on μRWELL data to compare with 5 sigma pedestal cut and demonstrate that this does not impact the efficiency of the prototype though it helps with the suppression of noisy strips and fake hits in the analysis. Moreover, we impose a minimum of 2-strip-with-hit criteria for the selection of good cluster, with each strip of the cluster with an ADC counts above pedestal threshold and the total cluster ADC counts ≥ 100 ADC counts. These two criteria were only applied to the μRWELL data. Applying these criteria helps with the spatial resolution analysis by removing fake hits but has no adverse impact on the efficiency or resolution of the prototype as we will show later in this paper. For the four triple-GEM detectors used as reference trackers, we applied a higher threshold of 7 sigma pedestal cut for zero suppression in order to eliminate any possibility of spurious tracks caused by noisy strips or cross talk for the track selection.

5.1. Cluster charge and X-Y charge sharing vs. HV

Fig. 6 shows the cluster charge distribution plots (in ADC counts) for x-strips (left) and y-strips (center). The cluster charge is defined as the sum of the ADC charge of all the strips in the cluster. For each strip in the cluster, the charges are integrated over all nine APV25 time samples. The charge sharing between x-strips and y-strips is shown on the correlation plot at the right, that is fitted to a straight line function showing a slope of 0.7916 ± 0.0013, meaning that x-strips (top strips) collect approximately 20% more charge than y-strips (bottom strips). The non-equal sharing indicates that the initial choice of the relative width for x- and y-strips as discussed in Section 3 is far from optimal and need to be revisited when designing the next capacitive-sharing μRWELL prototypes by slightly reducing the width of the top strips and conversely increasing the width of the bottom strips.

The mean cluster charge, defined as the most probable value (MPV) of the Landau function fitted to the data on x-strips (blue circle) and y-strips (red square) are plotted as a function of the HV on the μRWELL foil (left) and the electric field in the drift (right) in Fig. 7. In both plots, the data are shown for two pedestal cuts, $3\sigma_{ped}$ (circle) and $5\sigma_{ped}$ (square) respectively. The mean cluster charge is higher for x-strips than that of the y-strips as already discussed above. The mean cluster charge are also slightly higher for $3\sigma_{ped}$ as expected. The data for $5\sigma_{ped}$ cut on the left plot fit very well to an exponential function as expected from detector gain increase with the applied voltage to the μRWELL amplification structure. More interesting is the linear increase of the cluster charge as a function of the electric field in the drift region as shown in the plot in the right of Fig. 7. An linear increase of ~10% for both *x* and *y* strips is observed when the drift field varies from 1 kV/cm to 2 kV/cm. This result is consistent with the study reported in [3] on the charge collection efficiency of a μRWELL detector as a function of the drift field. We would expect from the study in [3] a plateau for the charge collection efficiency at about a drift field of 3 to 3.5 kV/cm.

5.2. Efficiency vs. HV

The detector efficiency along x- and y-strips is shown in Fig. 8 as a function of the HV on the μRWELL foil (left) and the electric field in the drift region (right). The efficiency for each axis is calculated by fitting the coordinate of the 4 GEM trackers along that axis and looking for the measured coordinate in the μRWELL prototype data within a 500 μm radius of the projected coordinate from the fitted track. The analysis is done at 3 and $5\sigma_{ped}$ cut. The efficiency exceeds (96 ± 1)% for both *x* and *y* strips at a voltage of 570 V applied on μRWELL amplification even at $5\sigma_{ped}$ cut as shown in the plot on the left and exceed (98 ± 1)% at 580 V.

The detector is fully efficient, ≥ (98 ± 1)%, at 575 V for both x-strips and y-strips even when the "2-strip minimum in the cluster" criteria is applied as it is the case for the data in the current study. This is another illustration of the unique feature of capacitive-sharing readout structures. The detection efficiency of a μRWELL detector with a conventional 800 μm-pitch 2D strip readout anode PCB, will drop significantly if the single-strip cluster events are removed from the analysis. Having the possibility to eliminate single-strip cluster events from the position reconstruction analysis without degrading the detector efficiency has two important advantages. The first is that it helps improving the spatial resolution performance of the detector because single-strip cluster are not sensitive to the center of gravity (COG) method used to accurately calculate the particle position coordinates. The second is that, removing single-hit event from the analysis is a very effective method to eliminate or substantially reduce the probability of fake hits or noisy channels from the reconstruction. The capacitive-sharing readout concept gives the flexibility to effectively control not only the strip multiplicity in the cluster but also and more importantly to ensure a minimum of 2-strip cluster for all good events, almost independently of the pitch of the strip readout structure and the size of the ionization charge cluster from the amplification device i.e. the chosen MPGD technology. This constitutes a big advantage compared to alternative approaches [12–14].

For the lowest HV setting at 550 V, the efficiency drops below (90.0 ± 0.6)% for *x* and (85.0 ± 0.6)% for y. The efficiency drop is more pronounced for y-strips as expected due to lower charge collection as discussed in Section 5.1. The plot in the right of Fig. 8, shows the efficiency curve as a function of the electric field in the drift region and a small linear increase with the drift field from 98.0 to 98.7% for y-strips and from 98.5 to 99.2% for x-strips is observed when the drift field increases from 1 to 2 kV/cm with a statistical error of ±0.4% in both cases.

5.3. Strip multiplicity vs. HV

Strip multiplicity, which is defined as the number of strips with hit in a cluster per event is a key parameter of the center of gravity (COG)

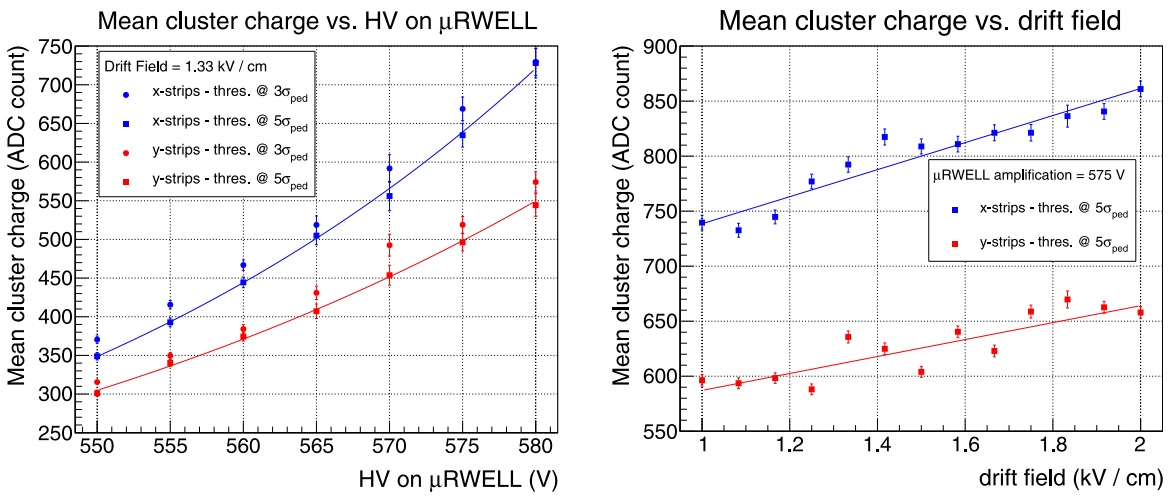

Fig. 7. *Left:* Mean cluster charge distribution in *x (blue)* and in *y (red)* as a function of the HV applied to the μRWELL foil for $3\sigma_{ped}$ cut *(circle)* and $5\sigma_{ped}$ cut *(square)*; the solid lines are fits to an exponential function. *right:* Mean cluster charge distribution in *x (blue)* and in *y (red)* as a function of the electric field in the drift region for $5\sigma_{ped}$ cut; the solid lines are fits to a straight line function.

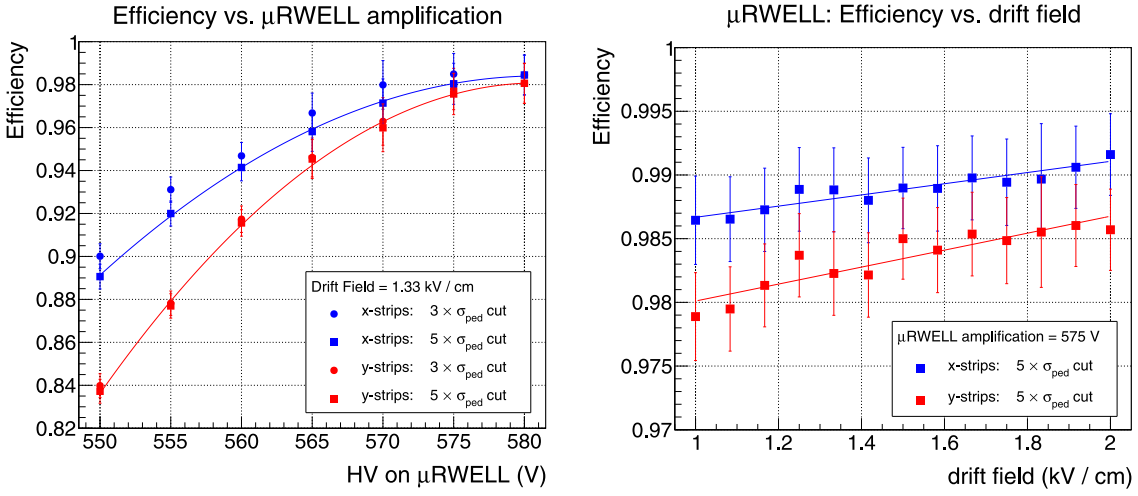

Fig. 8. *Left:* Efficiency in *x (blue)* and in *y (red)* as a function of the HV applied to the μRWELL foil for $3\sigma_{ped}$ cut *(circle)* and $5\sigma_{ped}$ cut *(square)*; the solid lines are fits to an exponential function. *right:* Detector efficiency in *x (blue)* and in *y (red)* as a function of the electric field in the drift region for $5\sigma_{ped}$ cut; the solid lines are fits to a straight line function.

method used for the reconstruction of the particle positions in MPGDs. A good spatial resolution requires a minimum of three strips on average in the cluster. Fig. 9 shows the distribution of the number of strips in the clusters in *x* (left) and in *y* (right) at $5\sigma_{ped}$ pedestal cut, for a drift field of 1.33 kV/cm and a voltage μRWELL foil equal to 580 V. The strip multiplicity, extracted from the mean value of Gaussian fit to the distributions is ∼ 4.04± 0.03 for both x-strips and y-strips.

Fig. 10 shows on the left plot, the strip multiplicity for x-strips (blue dots) and y-strips (red dots) as a function of the voltage applied to the μRWELL electrode for two threshold levels 3 and $5\sigma_{ped}$ for the zero suppression. at a $5\sigma_{ped}$ pedestal cut, the strip multiplicity increases linearly from 3.30 to 4.04 ± 0.03 for both *x* and *y* axis as the voltage is increased from 550 to 580 V. Even at lower gain for the lowest voltage of 550 V on the μRWELL foil, the strip multiplicity is higher than three for a readout pitch of 800 μm. We also observe in the right plot of Fig. 10 a linear increase of the strip multiplicity from ∼4.05 to ∼4.20 strips ± 0.01 in both *x* and *y* when the electric field in the drift region increases from 1 to 2 kV/cm. The data shows a strip multiplicity larger than three strips for large ranges of detector gain and drift field which ensures a good position resolution performance as shown in Section 6. The results demonstrates the characteristic feature of capacitive-sharing readout structures, in full agreement with the observation made in Section 5.2 regarding the 2-strip minimum per cluster criteria.

5.4. Timing performance of capacitive-sharing readout

It has been reported that for resistive-sharing readout structures [14–16], a significant time delay is observed between the signal of the central strip in the cluster and its neighboring strips. The difference in the measured peaking time of the signal on the front end (FE) pre-amplifier of the central strip and the first neighboring strip is typically a few hundreds ns and can be as large as 1 μs. Moreover, the time difference varies significantly with the charge amplitude ratio between the central strip and its neighbors. This time delay combined with the dependence on the charge sharing ratio would severely limit the detector performance and rate capability even in a relatively moderate rate environment. This is because a large time window, $\mathcal{O}$(μs), would be required from a data acquisition system to capture the signal of all the strips contributing to the cluster. In addition, resolving pile-up effect and multiple hit ambiguity becomes even more challenging as the time correlation information can no longer be used as a reliable tool to identify hits of the same cluster events. To study the timing performance of μRWELL prototype with capacitive-sharing X-Y strip

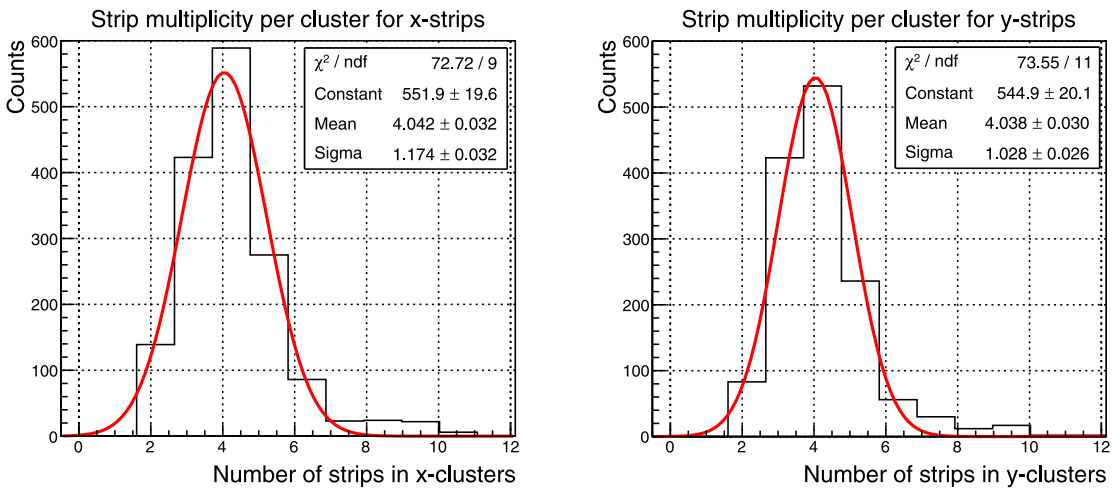

Fig. 9. *Left:* Strip multiplicity distribution in *x (blue)* and in *y (red)* for HV(μRWELL) = 575 V, drift field 1.33 kV and for $3\sigma_{ped}$; The distributions are fitted to a Gaussian function to obtain the strip multiplicity defined as the average number of strip per cluster for each HV setting.

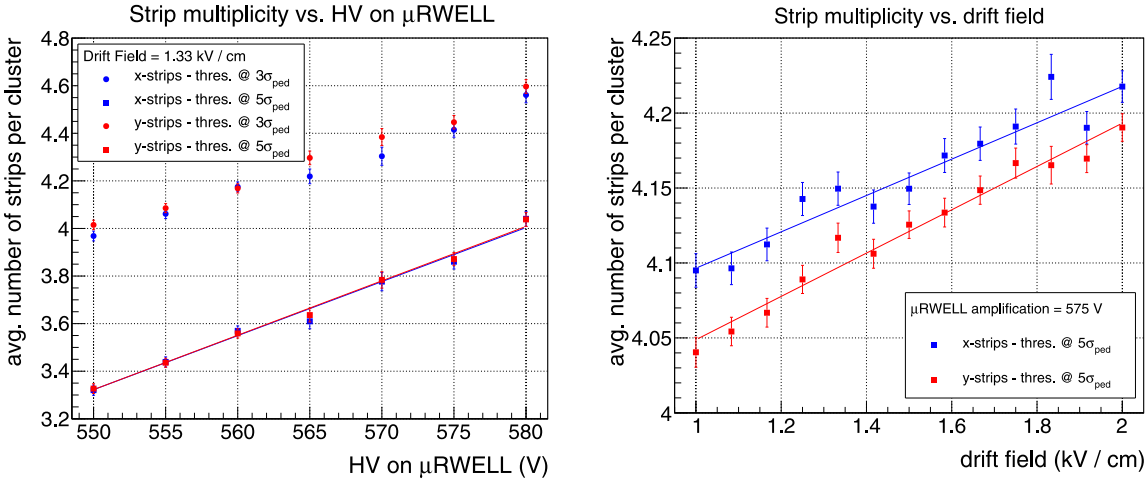

Fig. 10. *Left:* Mean strip multiplicity in *x (blue)* and in *y (red)* as a function of the HV on the μRWELL for $3\sigma_{ped}$ cut *(circle)* and $5\sigma_{ped}$ cut *(square)*; the solid lines are fits to an linear function. *Right:* Mean strip multiplicity in *x (blue)* and in *y (red)* as a function of the electric field in the drift region for $5\sigma_{ped}$ cut; the solid lines are fits to a linear function.

readout, we look at the timing correlation of neighboring strips of the same cluster. The first neighboring strips are defined as the two strips immediately at the left and right of the central strip and the second neighboring strips as the second set of strips (third and fourth strips) at the left and right of the central strip. The timing performance of the μRWELL prototype is compared to one GEM tracker with standard X-Y readout of the experimental setup.

The plots of Fig. 11 show a waveform shape of the digitized ADC time samples of APV25 signal from the μRWELL prototype (top plots) and the GEM tracker (bottom plots) for the *x* and *y* strips and for the central and first pair of neighboring strips for a typical triggered event. The digitized waveform signal fit perfectly with a Landau function and the most probable value (MVP) of the fit function is chosen as the APV25 signal peaking time with respect to the reference time t_0 defined as the first APV25 time sample. This reference time t_0 is the trigger latency (time delay) relative to the Hall D PS coincidence signal time used to trigger the APV25-SRS readout and is the same for all APV25 data. The distribution plots of the peaking time for a large data sample are shown in Fig. 12 for both the μRWELL prototype (top plots) and the GEM tracker (bottom plots). The mean value of the peaking time distributions of the central strip (left), the first neighboring strips (middle), and the second neighboring strips (right) are (60.47 ± 0.07) ns, (62.2 ± 0.1) ns and (57.36 ± 0.09) ns respectively, for the μRWELL prototype and (120.1 ± 0.1) ns, (116.8 ± 0.1) ns and (104.7 ± 0.1) ns for the GEM tracker. The width of the peaking time distributions of the central strip (left), the first neighboring strips (middle), and the second neighboring strips (right) are (15.98 ± 0.06) ns, (16.96 ± 0.06) ns and (19.94 ± 0.07) ns respectively, for the μRWELL prototype and (13.41 ± 0.04) ns, (14.11 ± 0.04) ns and (17.77 ± 0.06) ns for the GEM tracker. The width of the peaking time distributions is dominated by the APV25 time jitter of ∼12.5 ns [22] relative to the trigger signal. The slightly higher value of the width of the peaking time distributions compared to the 12.5 ns time jitter is due by the time walk contribution of individual strip. The difference of mean of the peaking time distribution between the central strip, its first and second neighbors is less than 2 and 3 ns respectively for the μRWELL prototype and less than 4 ns and 15 ns for the GEM tracker. The differences are well below the 12.5 ns APV25 time jitter (width of the distributions) for each set of strip, except for the second neighboring strips of the GEM tracker. In addition the peaking time of the APV25 signal of the GEM tracker is shifted by ∼60 ns with respect to the μRWELL APV25 peaking time. The shift is due by the additional 3 × 2 mm transfer regions between the first two GEM foils and in the induction region between the third GEM foil and the readout plane, adding a total of 6 mm drift time for the charges in the GEM trackers to reach the anode when compared to the μRWELL prototype. The additional drift time of the charge associated with this 6 mm gap in an $Ar:CO_2$ (80:20) gas mixture and electric field of 3.5 kV/cm is about 90 ns. However, the

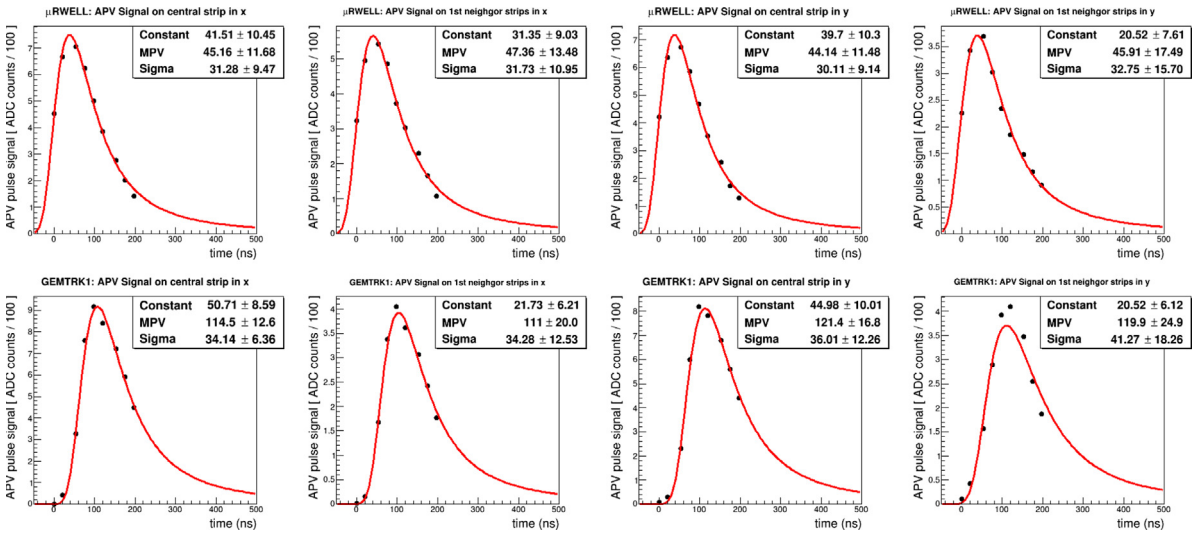

Fig. 11. APV25 waveform signal of strips in the cluster for the capacitive-sharing μRWELL prototype *(top)* and one GEM tracker *(bottom)* for a typical event: *(From left to right)*: APV25 waveform signal is shown for the central strip *(left)* and first neighbors (first strips on the left and right of the central strip) in the cluster for x *(middle left)*; for y *(right)* in the cluster.

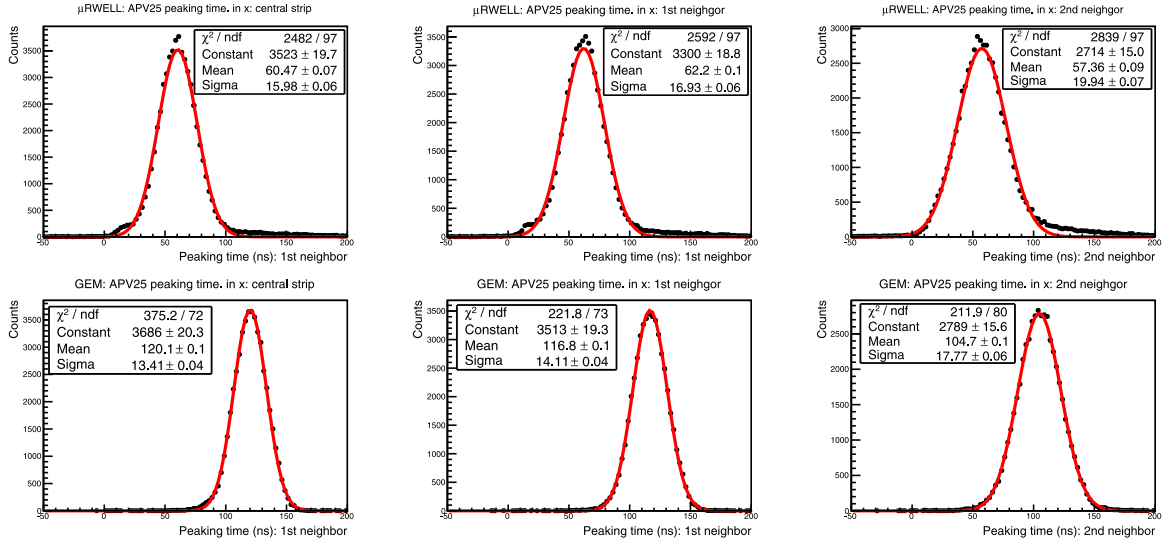

Fig. 12. APV25 signal peaking time distribution plots in x for the capacitive-sharing μRWELL prototype *(top)* and a GEM tracker *(bottom)* for the central strip *(left)*, the first two neighbors (first strips on the left and right of the central strip) *(middle)* and the second neighbors (second strips on the left and right of the central strip) *(right)* in the cluster.

electric field in the drift gap of the GEM is also higher (2.3 kV/cm) than in the μRWELL prototype (1.33 kV/cm) which reduces the time delay between the μRWELL prototype and the GEM tracker by about 15 ns. The expected time delay between the GEM and the μRWELL is about 75 ns. The 15 ns discrepancy observed between expected and measured delay is most likely due to other external factors such as the gas pressure inside the detectors as well as cabling of the electronics.

The 2D correlation plots of the peaking time of the central strip versus its first two neighbors are shown in Fig. 13 for the μRWELL prototype (top plots) and GEM tracker (bottom plots). The first two plots, starting from the left, show peaking time correlation between the central strip and its first neighbors in x and y axis respectively, and the last two plots show the correlation between the central strip and its second neighbors in x and y axis respectively. The 1D distribution plots of the difference in the timing between signal of the central strip and its first two neighbors are shown in Fig. 14. These plots show a small difference in the peaking time between strips of the same cluster event in the μRWELL detector. The highest difference is 4 ns between the central strip and its second neighbor for the x-strips and 2 ns difference between the central strip and its first neighbors for y-strips. The timing difference between the central strip and its first neighbor is three times worse the GEM trackers and is as high as 17 ns between the central strips and the second neighboring strips in both x and y axis. Also, these results show that external parameters are the cause of the small timing difference for these detectors and that capacitive-sharing readout structures induce only a small difference in time between the strips sharing the charge from the same event in a cluster.

The excellent timing performance of capacitive-sharing readout structures as compared with resistive readout structures can be attributed to the fact that the charge sharing mechanisms for these two structures are completely different. In resistive sharing readout, the resistive layer can be modeled as a resistive-capacitive network to the pad or strip readout plane. The lateral dispersion of a localized charge impinging the readout is governed by the RC time constant of the surface resistivity of the resistive layer. The propagation of the induced charge to the neighboring pads or strips from the central pad is defined by the RC time constant of the resistive layer. Consequently, a large acquisition time window is required for the readout electronics to capture the peaking time of the signal from different channels connected

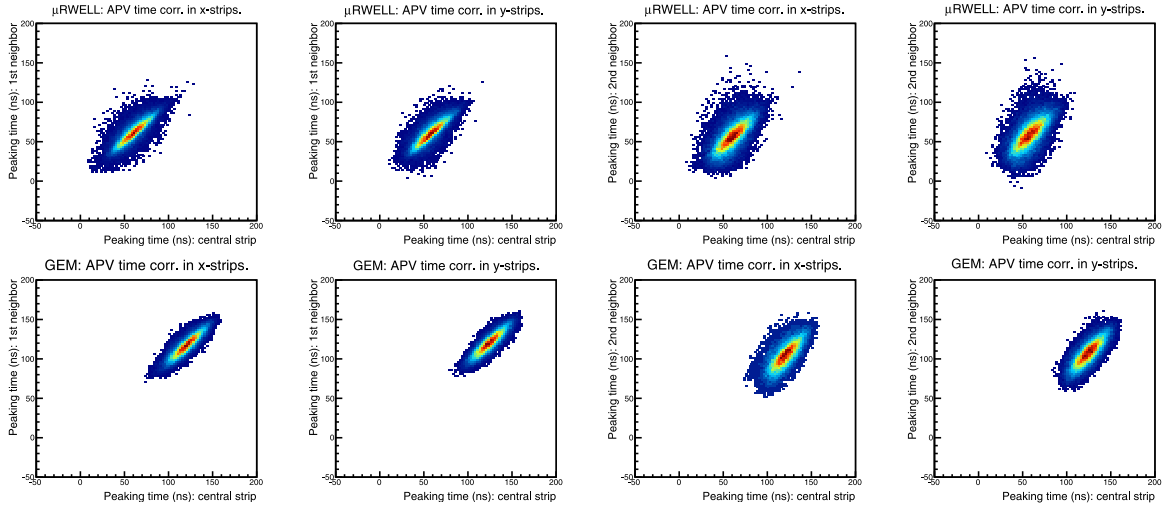

Fig. 13. APV25 signal peaking time correlation plots for the capacitive-sharing µRWELL prototype *(top)* and a GEM tracker *(bottom)*. *(From left to right)*: peaking time correlation between the central strip and its first neighbors (first strip on the left and right of the central strip) in *x (left)*, and in *y (middle left)*; and between the central strip and its second neighbors (second strips on the left and right of the central strip) in *x (middle right)* and in *y (right)* in the cluster.

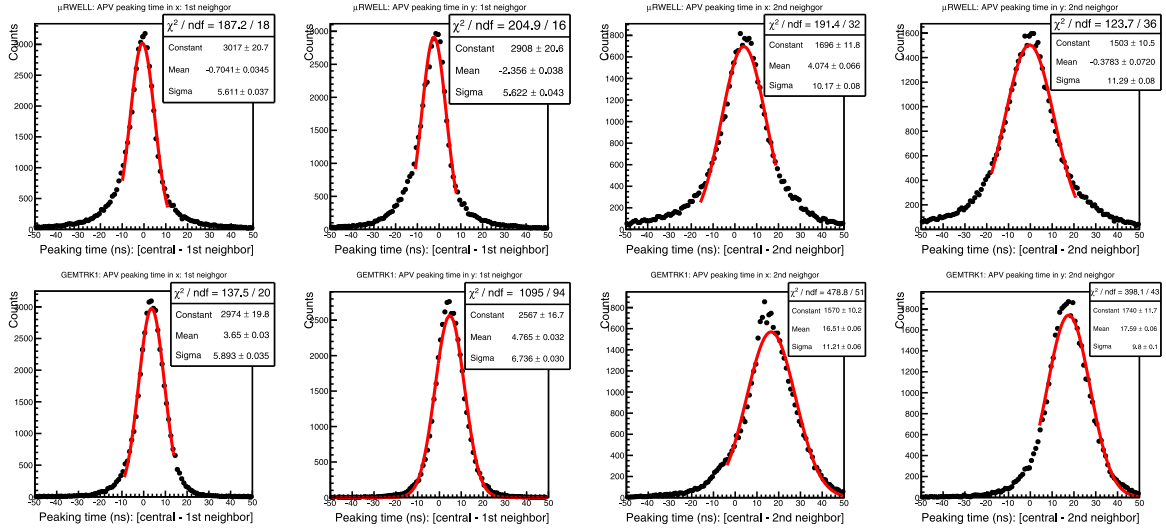

Fig. 14. APV25 signal peaking time difference for the capacitive-sharing µRWELL prototype *(top)* and GEM tracker *(bottom)*. *(From left to right)*: peaking time difference between the central strip and its first neighbors (two first strips on the left and right of the central strip) in *x (left)* and in *y (middle left)*; and between the central and its second neighbors (second strips on the left and right of the central strip) in *x (middle right)* and in *y (right)*.

to the pads of strips of the same cluster events. With capacitive-sharing readout, the signal propagates vertically at near the speed of light via capacitive coupling through the transfer layers of the PCB and the sharing of the charges over several strips is determined by the electric field configuration between pad along the vertical axis. No resistances are involved in the charge transfer process and therefore there is no time delay for charge collected and shared between strips of the readout layer.

6. Spatial resolution performance studies

As shown in Fig. 4 of Section 4, the beam test setup consists of four standard COMPASS GEM trackers, two upstream and two downstream of the µRWELL prototype under study, to allow a clean reconstruction of the electron tracks by requiring hits in both *x* and *y* axis of the four trackers for spatial resolution analysis of the prototype. The tracks are fitted using only the hit information from the trackers and excluding the hits from the µRWELL prototype.

6.1. Detector response linearity

The response linearity of the prototype is shown in the plots of Fig. 15. The linearity plots for x-strips (left) and y-strips (center right) show excellent correlation between measured coordinates in the detector and expected coordinates from the track fit. The 2D distribution of the track fit residuals are shown in the center left plot for x-strips and at the right for y-strips. No differential nonlinearity is observed, indicating a good and continuous response uniformity of the detector over the full active area. The few vertical occupancy gaps in the x-coordinate plot are caused by dead channels in the APV25 front end cards used to read out both the µRWELL prototype as well as the GEM trackers. Since we require hits in all four trackers for a good event, missing hits from dead

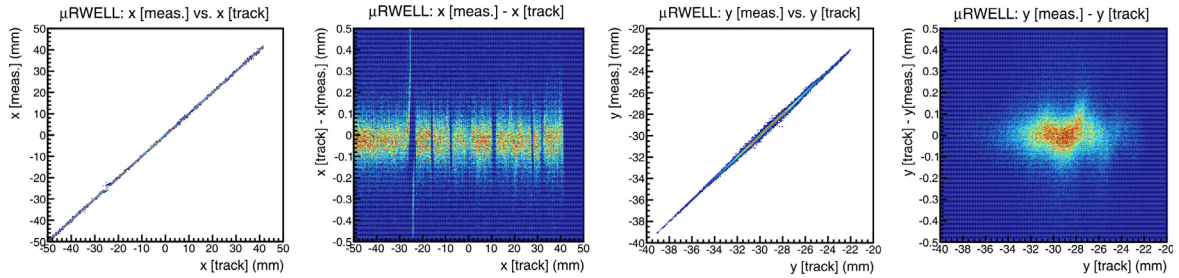

Fig. 15. *Left:* Correlation between expected and measured coordinates in x *(left)*; 2D distribution of the track fit residuals in x *(center left)*; Correlation between expected and measured coordinates in y *(center right)*; 2D distribution of the track fit residuals in y *(right)*.

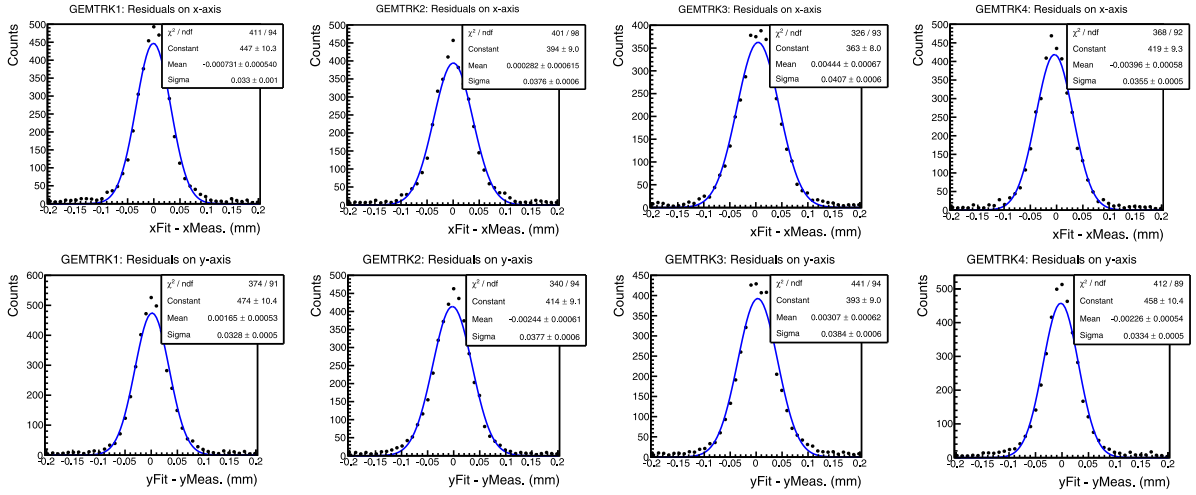

Fig. 16. Track fit residual distribution plots for all four GEM trackers in x *(top)* and y *(Bottom)*.

channels from the trackers electronics will reflect as occupancy gaps in the μRWELL data. The low occupancy gap at the left of the plots is a bad channel of the μRWELL prototype readout electronics as also observed in the hit position distribution plots of Fig. 5.

6.2. Track fit residuals

The first step of the analysis of the spatial resolution performance of the μRWELL prototype, is to estimate the contribution to the track fit error due to the finite resolution of the GEM trackers and to subtract in quadrature this error from the width (σ) of the Gaussian function fit of the μRWELL residual distributions. To that effect, we develop a simple ROOT script that simulates the beam test setup and produces tracks reproducing the Hall D PS electron beam characteristics in term of the angular and position distributions along both x and y axis.

The coordinates (x_i^{true}, y_i^{true}) of the projected "true" tracks at the z_i location of each of the four GEM trackers Trk_i are smeared with a Gaussian distribution with a width equal to nominal spatial resolution of tracker σ_i. The smeared coordinates (x_i^{smear}, y_i^{smear}) are then fitted to a straight line function. The residual distributions (x_i^{fit} - x_i^{smear}) and (y_i^{fit} - y_i^{smear}) are extracted and compared with the residual distribution of the trackers data from fitted tracks using these same trackers data. The input spatial resolution σ_i of each tracker used as input in the ROOT script for the "true" tracks is tuned to match the output of the residual distributions from simulated data shown in Fig. 17 with the residual distributions from the beam test data shown in Fig. 16. In both Figs. 16 and 17, the plots on top show the residual distributions in x for all four trackers and the bottom plots show the residual distributions in y. The input spatial resolution was set to 45 μm for each tracker.

The width of the track fit residuals $\sigma_i^{fit}(x)$ and $\sigma_i^{fit}(y)$ varies from 33 to 40 μm, for both real and simulated data. From these results, we can now extract the error expected from the fitted tracks at the z location of the μRWELL in the beam test setup. The track fit error is defined as the width σ^{err} of the Gaussian fit to the residual distributions ($x^{true}_{\mu RWELL}$ - $x^{fit}_{\mu RWELL}$) and ($y^{true}_{\mu RWELL}$ - $y^{fit}_{\mu RWELL}$), calculated from the projected coordinates at $z_{\mu RWELL}$ of the "true" tracks (assuming the trackers spatial resolution is equal to 0) and the fitted tracks from the smeared coordinates of the trackers. For both "true" and fitted tracks, the spatial resolution of the μRWELL prototype is set to zero for the purpose of finding the track fit error. The residual distribution plot of the track fit error is shown in Fig. 18. The plots show (21.2 ± 0.6) μm and (20.6 ± 0.6) μm for the widths σ_x^{err} and σ_y^{err} of the narrower Gaussian function of the double Gaussian fit to the distributions respectively.

6.3. Spatial resolution performance of the μRWELL prototype

The plots of Fig. 19 show the residual distributions of fitted tracks in the x and y axis, respectively, of the μRWELL prototype. The detector operates at a voltage setting of 575 V and a drift field of 1.33 kV/cm. The widths of the narrower Gaussian function of double Gaussian fits to the residual distributions are σ_x^{res} = (63.1 ± 1.0) μm and σ_y^{res} = (62.6 ± 1.0) μm for x-strips and y-strips, respectively. The spatial resolutions in x and y axes are calculated by subtracting in quadrature the track fit error σ_x^{err} and σ_y^{err}, discussed in Section 6.2, from the width of the residual distributions, respectively, as shown in Eq. (1).

$$\sigma_x^2 = (\sigma_x^{res})^2 - (\sigma_x^{err})^2$$
$$\sigma_y^2 = (\sigma_y^{res})^2 - (\sigma_y^{err})^2 \quad (1)$$

Fig. 20 shows an example of the residual widths $\sigma^{res}_{x(y)}$ (red dots) and the calculated spatial resolutions $\sigma_{x(y)}$ after track fit error subtraction (blue dots) for 16 independent runs for x-strips (left plot) and y-strips (right plot). The mean value of the σ width of the Gaussian fit to the

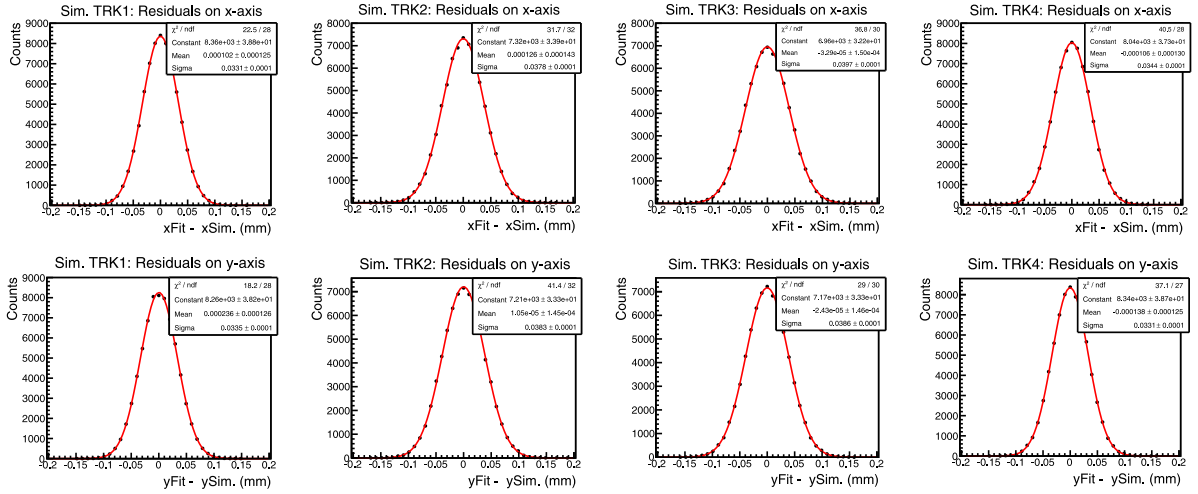

Fig. 17. Simulated track fit residual distribution plots in for all four GEM trackers in *x (top)* and *y (Bottom)*.

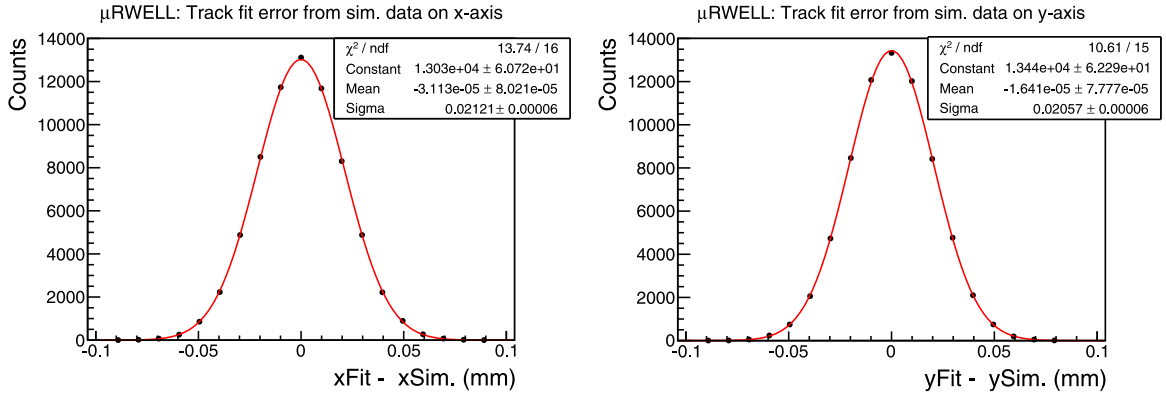

Fig. 18. Simulated track fit residual distribution plots at the z location of the μRWELL prototype in *x (left)* and *y (right)*. The width of the Gaussian fit to the distribution represents the track fit error σ^{error}.

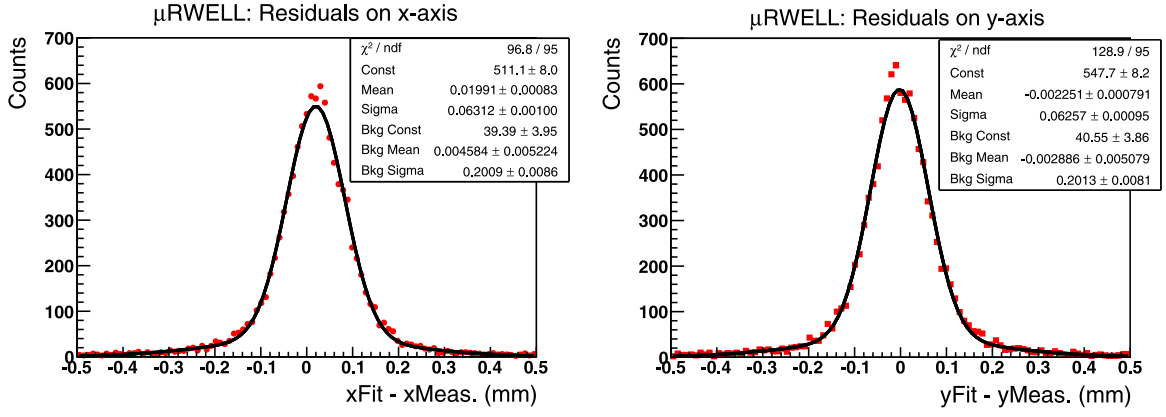

Fig. 19. μRWELL residual distribution plots in *x (left)* and *y (middle)* for HV = 575 V and drift field = 1.33 kV/cm.

residuals over 16 runs is σ_x^{res} (mean) = 64.61 μm and σ_y^{res} (mean) = 64.09 μm with ∼2 μm fluctuation from run to run. The mean value of the calculated spatial resolution is σ_x (mean) = 61.03 μm and σ_y (mean) = 60.69 μm. The contribution of the track fit error σ^{err} to spatial resolution in both *x*-axis and *y*-axis is in the order of ∼ 3.5μm.

We looked at the spatial resolution performance of the μRWELL prototype as a function of the voltage applied to the μRWELL foil and the electric field in the drift region. The plot in the left of Fig. 21, shows a clear dependence of the spatial resolution on the detector gain and a steady improvement of the resolution, that is, a decrease of the resolution from 80 μm to 60 μm when the voltage applied to μRWELL foil increases from 550 to 580 V. This result is very interesting as it shows that even with 550 V applied to the μRWELL foil which corresponds to a gain of ∼ 4.5×10^3 [3], and with the efficiency dropping below 90%, the spatial resolution which is equal to 82 μm is still well below 100 μm for an 800 μm pitch strip readout. The spatial resolution improves by 20 μm when the voltage on the μRWELL foil increases by 30 V which corresponds to a gain increase by a factor of

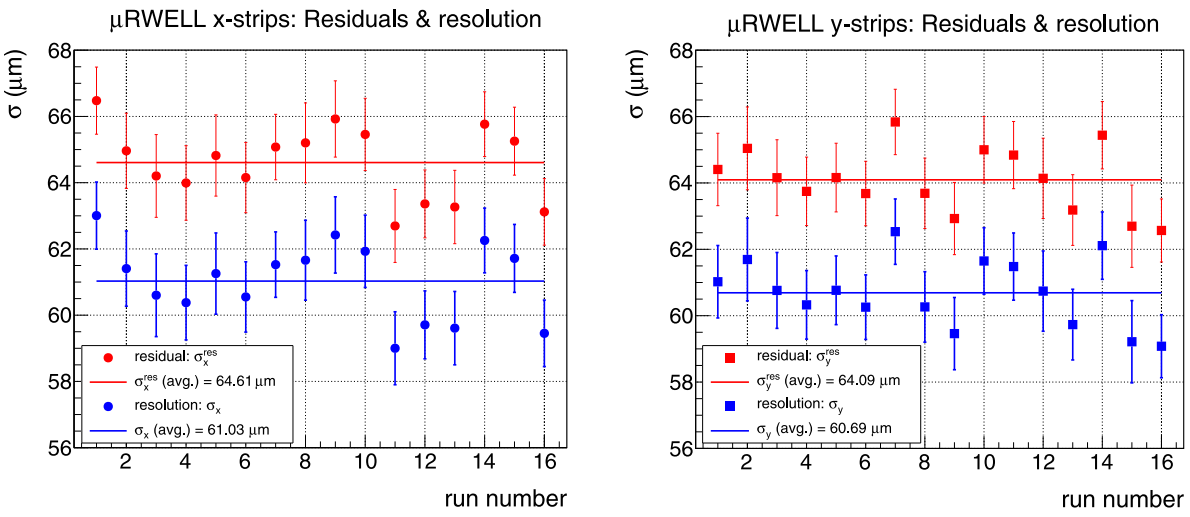

Fig. 20. Widths ($\sigma_{x,y}^{res}$) of the Gaussian fit to the residuals in *(red)* and spatial resolution ($\sigma_{x,y}$) after track fit error correction *(blue)* in *x (left)* and in *y (right)* for 16 independent runs at HV = 575 V and drift field = 1.33 kV/cm. The mean values $\sigma_{x,y}^{res}$ (mean) and $\sigma_{x,y}$ (mean) are also shown as horizontal line on the plots.

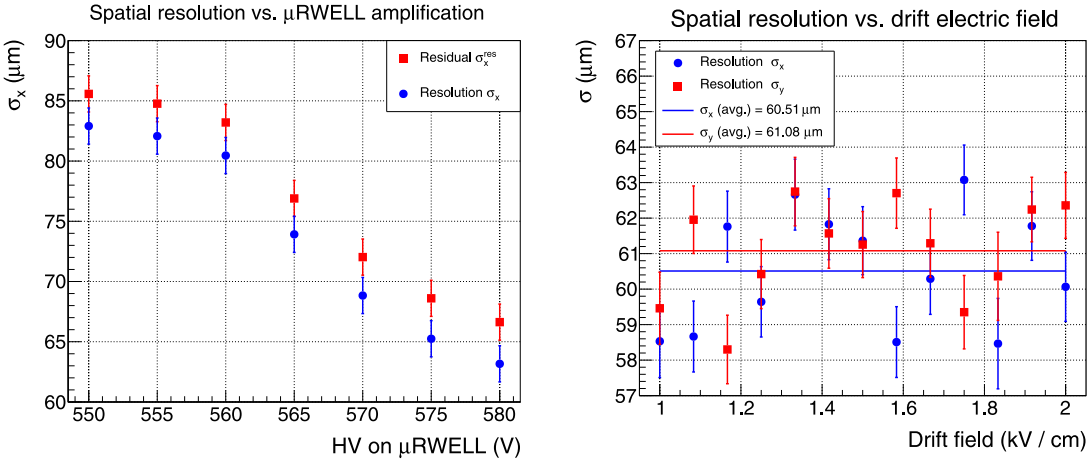

Fig. 21. *Left:* Spatial resolution in x-strips as a function of HV on the µRWELL foil; *Right:* Spatial resolution in *x (blue)* and in *y (red)* of µRWELL prototype as a function of the electric field in the drift region of the prototype.

2 as shown in Fig. 7. The mild dependence of the spatial resolution on the voltage applied to the µRWELL foil i.e. detector gain is a feature of the capacitive-sharing structure and an advantage over the alternative such as zigzag or resistive-sharing readout structures. This feature allows more flexibility with operating voltage defining the gain without compromising too much on the spatial resolution performances. The HV scan run was performed at the beginning of the beam test and unfortunately there was a mistake in the configuration of the APV25-SRS electronics connected to the y-strips of all four GEM trackers used for the fit. For this run, data were not available to fit the tracks in *y* axis and extract the spatial resolution on y-strips as a function of the HV on the µRWELL foil. Fig. 21 shows the spatial resolution plots for x-strips only. However, as shown in the plots of Fig. 19, the expected spatial resolution performance in y-strips is similar to the x-strips, within 1 or 2 µm fluctuations. In the right of Fig. 21, the plots show that spatial resolution is basically independent of the electric field in the drift region of the detector within the range of 1 to 2 kV/cm. The resolution is equal to 60.51 µm on average for both x-strips and 61.08 µm for y-strips with ∼2 µm fluctuation and in very good agreement with the observation of Fig. 20. These results are further evidence that capacitive-sharing structures have a very mild dependence on the parameters defining the charge amplification in MPGD structures and provide a high level of flexibility for optimization and operation of these detectors.

7. New capacitive-sharing readout structures

7.1. Development of 3-coordinates capacitive-sharing (x-y-u)-strip readout

Operating large MPGD tracking detectors with strip readout in high rate environments requires addressing issues of pile up and multiple hit ambiguity. The situation becomes even more critical with the development of low channel count readout structures with larger strip pitches. One obvious solution to address both multiple hit ambiguity and pile up effects is the development of 3-coordinate (x-y-u, u-v-y, ...) strip readout structures on a single PCB anode readout to enhance tracking capability in a high background rate environment. These 3-coordinate readout structures, when combined with fast electronics, are expected to combine time and amplitude of the charge shared by the strips in all three coordinates axes together with space information of the hit to precisely reconstruct the hit position, limit the impact of multiple hit ambiguity and pile-up as well as to help with background rejection. However, the main limitation so far to developing 3-coordinate strip readout on large-area PCB emanates from the fabrication of the devices. In fact, current fabrication techniques of 3-coordinate strip readout on standard PCBs requires a minimum strip pitch of 600 µm in order to preserve the spatial resolution performances. Even with this requirement, fabrication of 3-coordinate strip readout PCB remains extremely challenging with small size detectors and impractical for large-area

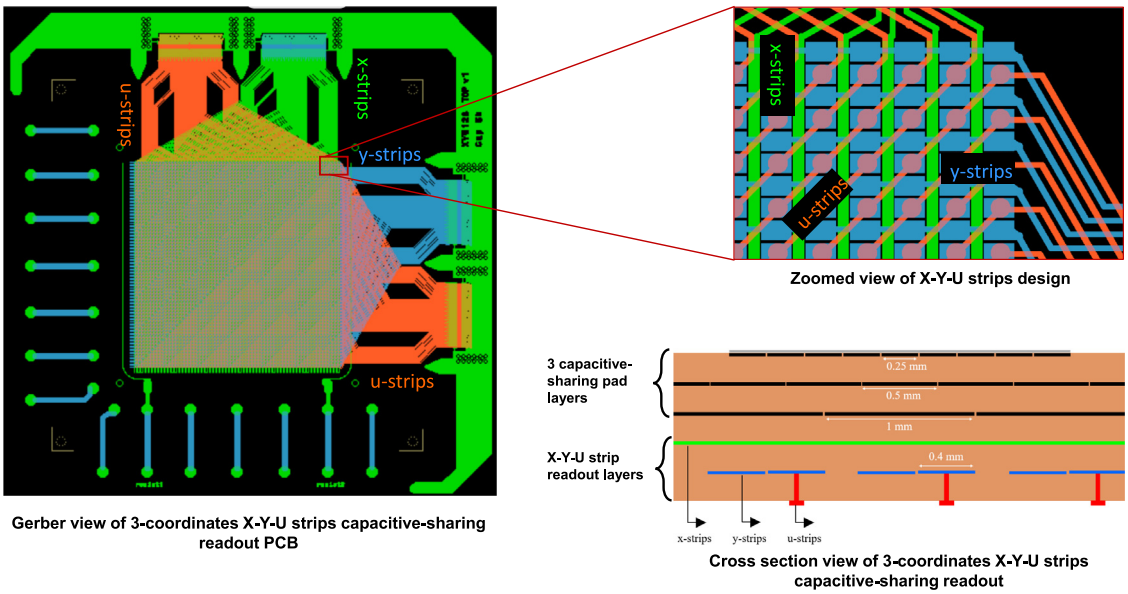

Fig. 22. Design of the 3-coordinates capacitive-sharing, 1 mm pitch, (x-y-u)-strip readout. *Left:* Gerber view of the (x-y-u)-strip readout PCB prototype; *top right:* Zoomed-in view of the readout active area with the x,y and u strip configuration and routing; *bottom right:* cross sectional view of the readout structures showing triple stack of capacitive-sharing pad layers and 2-layer readout for the x, *y* and u strips.

PCBs. In addition, a standard 3-coordinate strip readout PCB requires a large density of metallized vias with a multi-layer PCB process for connecting the strips to external connectors. Capacitive-sharing readout structures have the potential to overcome these technical limitations and allow the fabrication of cost effective, high-performance, large-area, 3-coordinate strip readout structures with strip pitch on the order of 1 to 2 mm and expected spatial resolution performances better than 100 μm. The first prototype of a 3-coordinates capacitive-sharing (x-y-u)-strip readout PCB was designed and is currently under fabrication. The design characteristics of the readout are shown in Fig. 22. The pitch of the strips is 800 μm. The x-strips, highlighted in green in Fig. 22 are on the first readout layer below the last capacitive-sharing transfer pad layer, and y-strips and u-strips are on a second layer below. The x-strips and y-strips are both straight strips while the u-strips are a set of pads that are interconnected through metallized vias along the diagonal axis to traces running on a third layer below; these traces carry the signal to the front-end electronics. This first 3-coordinates capacitive-sharing (x-y-u)-strip readout prototype will be tested with triple-GEM amplification to establish the proof of principle. We will subsequently develop a second prototype with 1 mm pitch and a μRWELL amplification.

7.2. Minimization of the capacitance noise

The input capacitance of the readout strips connected to the front end electronics should be kept as low as possible to minimize the capacitance noise at the FE and maximize the signal-to-noise ratio. This requirement presents a real challenge to any type of strip readout structures with large pitch, including zigzag or resistive-sharing readout and capacitive-sharing structures. In the case of capacitive-sharing readouts however, there is an easy solution for the large input capacitance noise problem. In fact, for capacitive-sharing readout structures the pitch of the strips or pads rather than the actual width of the strips or size of the pads is the key parameter for high-performance and low channel counts. This is because, unlike zigzag or resistive-sharing readout [13,15,16,18], for capacitive-sharing readout structures, the charge sharing between neighboring strips or pads does not require narrow inter-strips or inter-pads gaps. With narrower strips of smaller pad size, the collected signal is expected to be smaller, however, the signal amplitude can be compensated by an increase of the detector gain in order to maintain the charge sharing properties between strips or pads, regardless of the size of the pads or the width of the strips with respect to the pitch. This key feature of capacitive-sharing readout structure is expected to be maintained for low capacitance, large strips (or pads) anode readout PCBs for large MPGD detectors. In addition, with a larger inter-strip or inter-pad gaps, the cross-talk induced by inter-strip capacitance [23] would be greatly reduced. The cartoon sketch on the left of Fig. 23 shows the ideas for a low capacitance X-Y strip capacitive-sharing readout design, with a 2 mm strip pitch for both x-strips (red) and y-strips (blue). The width of the strips is 500 μm which is four times smaller than the strip pitch. The green, magenta and light brown square at the top right corner represents the pad sizes of the pad-transfer layers of the readout scheme. The cartoon on the right shows a similar idea with a capacitive-sharing pad readout PCB with a pad pitch and size of 2 and 4 mm, respectively; the pad electrode area is four times smaller than the pitch area. In summary, the capacitive-sharing concept allows users to freely adjust pad size or strip width for a given segmentation pitch to the specific application requirements. We intend to test new triple-GEM and μRWELL prototypes with capacitive-sharing anode readout PCBs to validate the concept.

7.3. Minimization of the material thickness for capacitive-sharing readout structures

Finally, some applications require low mass, that is, low-radiation-length tracking detectors to minimize multiple Coulomb scattering in order to achieve good position and momentum resolution performance. R&D efforts [9,17] are ongoing to develop thin and low mass transfer pad layers for capacitive-sharing readout structures, by using 0.1 μm chromium pads rather than the standard 5 μm Cu pads and by reducing the thickness of the dielectric layers by a factor of 2 to 4. A low mass μRWELL prototype with a thin layer Cr-based capacitive-sharing readout structure is under development to validate the idea.

8. Summary and outlook

Large-area MPGD trackers are being considered for several future NP and HEP experiments due to the many advantages (low cost, high spatial resolution, and high rate capabilities), offered by these technologies for large scale particle physics experiments. The capacitive-sharing

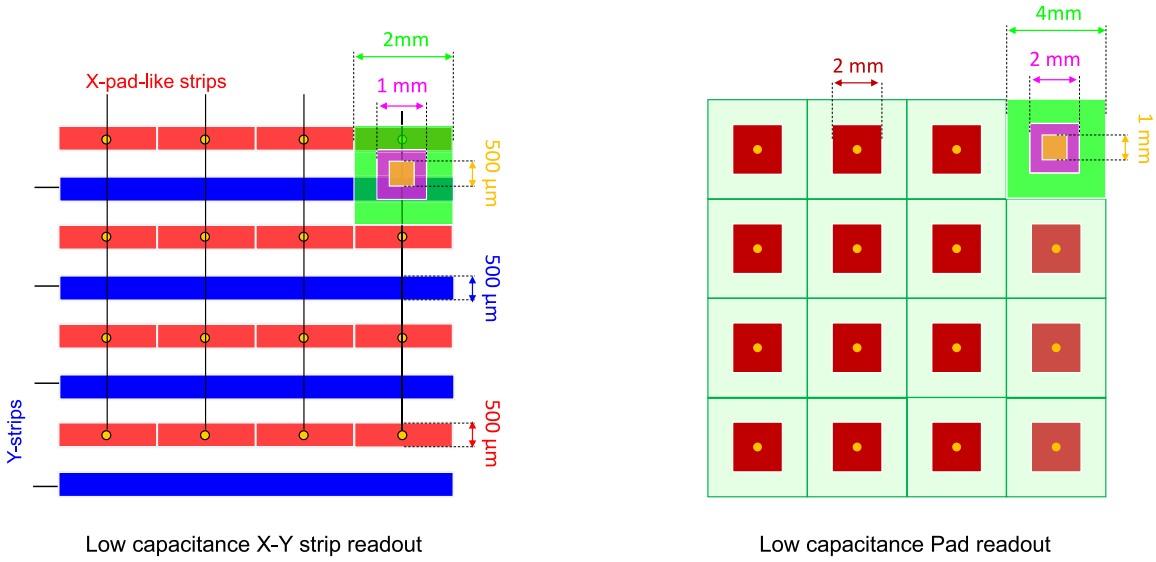

Fig. 23. Two design implementations of capacitive-sharing readout structures with low capacitance x-y strips on left and low capacitance pad readout on the right.

readout is a new concept aimed at developing high-performance anode readout PCBs for MPGD amplification structures, with coarse segmentation (1 to 2 mm pitch for strip readout) to significantly reduce readout electronics channel count and hence the cost of readout electronics. The concept of capacitive-sharing is based on a special spatial arrangement of metallic pads between dielectric layers in a vertical stack of these layers that allows the transfer of the induced charge signal from the MPGD amplification through capacitive coupling between the pad layers to the coarsely segmented pick-up strip (or pad) electrodes of the anode readout PCB of the detector. Capacitive-sharing readout structures open the possibility for the development of cost effective large-area tracking detectors with reduced number of channels while maintaining excellent spatial resolution performance. A μRWELL prototype with capacitive-sharing 2D strip anode readout PCB was developed in collaboration with the CERN PCB workshop group as a proof of concept. The prototype was based on a standard μRWELL amplification structure and a 3 mm drift gap combined with X-Y strip readout with a strip pitch of 800 μm and was successfully tested in the electron beam of the Pair Spectrometer setup in experimental Hall D at Jefferson Lab. A detector efficiency better than (98 ± 1) % was achieved. A spatial resolution performance in both x-strips and y-strips of the order of (60 ± 1) μm was achieved and is comparable to the performance of a standard triple-GEM detector with 400 μm pitch X-Y strip readout. The spatial resolution performance shows only moderate dependence over a large range with the voltage on the amplification structure, which is correlated with the μRWELL detector gain. No significant dependence of the spatial resolution performance on the electric field in the drift region was observed within a range of 1 to 2 kV/cm. The results also show a timing difference smaller than (6.00 ± 0.04) ns between neighboring strips of the same cluster which is less than the time jitter of the APV25 FE electronics. This is an indication that the capacitive-sharing readout structure does not introduce time delay between signal of neighboring strips sharing the charges. Future prototypes are under development to further study the capabilities of capacitive-sharing readout for MPGDs. These ongoing R&D efforts include the development of low mass, low noise strip readout structures for large-area MPGD trackers, with the development of a 3-coordinate (X-U-U or U-V-Y) strip readout configuration for suppression of multiple hit ambiguity and the mitigation of the pile-up impact on tracking in high background rate environments. In summary, capacitive-sharing readout structure is a very promising option for cost effective, high-performance large-area MPGD trackers for future nuclear physics experiments such as at Jefferson Lab or future collider experiments such as at the electron–ion collider (EIC) at Brookhaven National Laboratory.

Declaration of competing interest

The authors declare that they have no known competing financial interests or personal relationships that could have appeared to influence the work reported in this paper.

Data availability

No data was used for the research described in the article.

Acknowledgments

This work was supported by the site-neutral generic detector R&D program administered by BNL for the EIC, USA under the eRD6 program. The prototype was tested in beam in Hall D at Jefferson Lab. We would like to thank the lab and Hall D managements (in particular D. Higinbotham and E. Chudakov) for their continuing support and the technical team for the tremendous help in integrating our test setup in the Hall D test beam area. Finally I woud like to thank Ms Anzizath Yessoufou for her unwavering and warm support all these years.

References

[1] F. Sauli, GEM: A new concept for electron amplification in gas detectors, Nucl. Instrum. Meth. A386 (2) (1997) 531–534, http://dx.doi.org/10.1016/S0168-9002(96)01172-2, URL https://www.sciencedirect.com/science/article/pii/S0168900296011722.

[2] Y. Giomataris, P. Rebourgeard, J. Robert, G. Charpak, MICROMEGAS: A high-granularity position-sensitive gaseous detector for high particle-flux environments, Nucl. Instrum. Methods Phys. Res. A 376 (1) (1996) 29–35, http://dx.doi.org/10.1016/0168-9002(96)00175-1, URL http://www.sciencedirect.com/science/article/pii/0168900296001751.

[3] G. Bencivenni, R.D. Oliveira, G. Morello, M.P. Lener, The micro-resistive WELL detector: A compact spark-protected single amplification-stage MPGD, J. Instrum. 10 (02) (2015) P02008, http://dx.doi.org/10.1088/1748-0221/10/02/p02008.

[4] R. Chechik, A. Breskin, C. Shalem, D. Mörmann, Thick GEM-like hole multipliers: Properties and possible applications, Nucl. Instrum. Methods Phys. Res. A 535 (1) (2004) 303–308, http://dx.doi.org/10.1016/j.nima.2004.07.138, URL http://www.sciencedirect.com/science/article/pii/S0168900204016663, Proceedings of the 10th International Vienna Conference on Instrumentation.

[5] C. Altunbas, M. Capeans, K. Dehmelt, J. Ehlers, J. Friedrich, I. Konorov, A. Gandi, S. Kappler, B. Ketzer, R.D. Oliveira, S. Paul, A. Placci, L. Ropelewski, F. Sauli, F. Simon, M. van Stenis, Construction, test and commissioning of the triple-GEM tracking detector for compass, Nucl. Instrum. Meth. A490 (1) (2002) 177–203, http://dx.doi.org/10.1016/S0168-9002(02)00910-5, URL http://www.sciencedirect.com/science/article/pii/S0168900202009105.

[6] K. Gnanvo, et al., Large size GEM for super bigbite spectrometer (SBS) polarimeter for hall A 12 GeV program at JLab, Nucl. Instrum. Meth. A782 (2015) 77–86, http://dx.doi.org/10.1016/j.nima.2015.02.017, arXiv:1409.5393.

[7] K. Gnanvo, et al., Performance in test beam of a large-area and light-weight GEM detector with 2D stereo-angle (UV) strip readout, Nucl. Instrum. Meth. A808 (2016) 83–92, http://dx.doi.org/10.1016/j.nima.2015.11.071, URL https://www.sciencedirect.com/science/article/pii/S0168900215014369.

[8] J.P. Chen, H. Gao, T.K. Hemmick, Z.E. Meziani, P.A. Souder, The SoLID Collaboration, A white paper on SoLID (Solenoidal large intensity device), 2014, arXiv:1409.7741.

[9] S. Stepanyan, et al., CLAS12 upgrade for high luminosity operations task force report, 2020, CLAS12 High Lumi Task Force, https://wiki.jlab.org/physdivwiki/images/a/a9/CLAS12_high_lumi.pdf.

[10] R.A. Montgomery, J.R.M. Annand, D. Dutta, C.E. Keppel, P. King, B. Wojtsekhowski, J. Zhang, Proposed measurement of tagged deep inelastic scattering in Hall A of Jefferson lab, AIP Conf. Proc. 1819 (1) (2017) 030004, http://dx.doi.org/10.1063/1.4977122.

[11] J. Adam, et al., Electron-ion collider at Brookhaven national laboratory: Conceptual design report, 2021, https://www.bnl.gov/ec/files/EIC_CDR_Final.pdf.

[12] C. Perez-Lara, S. Aune, B. Azmoun, K. Dehmelt, A. Deshpande, W. Fan, P. Garg, T.K. Hemmick, M. Kebbiri, A. Kiselev, I. Mandjavidze, M.L. Purschke, M. Revolle, M. Vandenbroucke, C. Woody, A comparative study of straight-strip and zigzag-interleaved anode patterns for MPGD readouts, IEEE Trans. Nucl. Sci. 69 (1) (2022) 50–55, http://dx.doi.org/10.1109/TNS.2021.3132946.

[13] A. Zhang, M. Hohlmann, B. Azmoun, M.L. Purschke, C. Woody, A GEM readout with radial zigzag strips and linear charge-sharing response, Nucl. Instrum. Meth. A887 (2018) 184–192, http://dx.doi.org/10.1016/j.nima.2017.12.074, arXiv:1708.07931, URL https://www.sciencedirect.com/science/article/pii/S0168900217314924?via%3Dihub.

[14] P. Colas, Charge spreading with a resistive-capacitive coating, 2020, New Horizons for TPCs, October 9 - 10, 2020, https://indico.cern.ch/event/889369/contributions/4011324/attachments/2118361/3564530/ChargeSpreading_PColas.pdf.

[15] M. Dixit, J. Dubeau, J.-P. Martin, K. Sachs, Position sensing from charge dispersion in micro-pattern gas detectors with a resistive anode, Nucl. Instrum. Methods Phys. Res. A 518 (3) (2004) 721–727, http://dx.doi.org/10.1016/j.nima.2003.09.051, URL http://www.sciencedirect.com/science/article/pii/S0168900203026822.

[16] D. Attie, et al., Performances of a resistive Micromegas module for the time projection chambers of the T2K near detector upgrade, Nucl. Instrum. Methods Phys. Res. A 957 (2020) 163286, http://dx.doi.org/10.1016/j.nima.2019.163286, URL http://www.sciencedirect.com/science/article/pii/S0168900219315426.

[17] eRD108, EIC MPGD needs and R&D Strategies, 2021, CERN Experimental Physics R&D Day, https://indico.cern.ch/event/1063927/contributions/4560105/subcontributions/356566/attachments/2344971/3998579/eRD108_CERN-EIC-RD.pdf.

[18] Azmoun, et al., Design studies of high resolution readout planes using zigzags with GEM detectors, IEEE Trans. Nucl. Sci. PP (2020) 1, http://dx.doi.org/10.1109/TNS.2020.3001847, URL https://ieeexplore.ieee.org/document/9115073.

[19] M. French, L. Jones, Q. Morrissey, A. Neviani, R. Turchetta, J. Fulcher, G. Hall, E. Noah, M. Raymond, G. Cervelli, P. Moreira, G. Marseguerra, Design and results from the APV25, a deep sub-micron CMOS front-end chip for the CMS tracker, Nucl. Instrum. Meth. 466 (2) (2001) 359–365, http://dx.doi.org/10.1016/S0168-9002(01)00589-7, URL http://www.sciencedirect.com/science/article/pii/S0168900201005897, 4th Int. Symp. on Development and Application of Semiconductor Tracking Detectors.

[20] S. Martoiu, H. Muller, J. Toledo, Front-end electronics for the scalable readout system of RD51, in: 2011 IEEE Nuclear Science Symposium Conference Record, 2011, pp. 2036–2038, http://dx.doi.org/10.1109/NSSMIC.2011.6154414, URL https://ieeexplore.ieee.org/document/6154414/authors#authors.

[21] ALICE DAQ Projects, ALICE DAQ and ECS Manual, ALICE Internal Note DAQ ALICE-INT-2010-001 (2010).

[22] M. Phipps, SRS timing jitter: More clarity, 2015, EIC Tracking R&D (eRD6 - eRD108) bi-weekly meetings, https://wiki.bnl.gov/eic/upload/SRSTimingJune1.pptx.

[23] M. Abbas, et al., Interstrip capacitances of the readout board used in large triple-GEM detectors for the CMS muon upgrade, J. Instrum. 15 (12) (2020) P12019, http://dx.doi.org/10.1088/1748-0221/15/12/p12019.